Synthesis-Controlled Polymorphism and Anion Solubility in the Sodium ion-conductor $Na_3InCl_{6-x}Br_x$ ($0 \leq x \leq 2$)

Tong Zhao[a,b], Marvin A. Kraft[c], Wolfgang G. Zeier*[a,c]

[a]*Institute of Inorganic and Analytical Chemistry, University of Münster, 48149 Münster, Germany.*

[b]*International Graduate School of Battery Chemistry, Characterization, Analysis, Recycling and Application (BACCARA), University of Münster, 48149 Münster, Germany.*

[c]*Institut für Energie- und Klimaforschung (IEK), IEK-12: Helmholtz-Institut Münster, Forschungszentrum Jülich, 48149 Münster, Germany.*

*wzeier@uni-muenster.de

Abstract

Motivated by the significant transport property improvement of the anion substituted lithium metal halides, a series of anion mixed solid solutions of $Na_3InCl_{6-x}Br_x$ ($0 \leq x \leq 2$) is successfully synthesized by ball milling and subsequent annealing. By milling, the $Na_3InCl_{6-x}Br_x$ solid solution series crystallizes in a monoclinic $P2_1/n$ phase, while the subsequently annealed $Na_3InCl_{6-x}Br_x$ series transforms into a trigonal $P\bar{3}1c$ phase. By annealing and changing the structure type, a greater anion solubility can be achieved. The halide substitution slightly improves the ionic conductivity in the $Na_3InCl_{6-x}Br_x$ series, indicating that mixed-halide compositions and their structural changes affect the ionic transport albeit less strongly than in the lithium analogues such as $Li_3YCl_{6-x}Br_x$ and $Li_3InCl_{6-x}Br_x$.

Introduction

Sodium all-solid-state batteries have attracted growing interest in recent years because of their potentially high energy densities and superior safety in comparison to conventional sodium ion batteries employing liquid electrolyte.[1, 2] In addition, the abundance of sodium enables sodium all-solid-state batteries less costly than lithium solid-state batteries.[3, 4] All-solid-state batteries require solid electrolytes with high ionic conductivity, low electronic conductivity, excellent mechanical compatibility with the active materials and a wide electrochemical stability window.[5] So far, sulfide-based Na^+ conductors (e.g. Na_3PS_4) and oxide-based Na^+ conductors (e.g. NASICON) have been most widely explored to meet these requirements.[6-16] For instance, tungsten substituted Na_3SbS_4 ($Na_{2.9}Sb_{0.9}W_{0.1}S_4$) can be simply synthesized by solid reaction at 550 °C and exhibits an ionic conductivity of up to 4.1×10^{-2} S·cm^{-1} at room temperature.[17] Moreover, good mechanical strength and flexibility enable the sulfide-based sodium solid electrolyte to be mechanically compatible with the electrode volume change during charging/discharging.[2] However, their low oxidation stability and poor compatibility with sodium metal do not favor their practical application.[1, 2] In contrast, Sc-substituted NASICON $Na_{3.4}Sc_{0.4}Zr_{1.6}(SiO_4)_2(PO_4)$ exhibits an ionic conductivity of up to 4×10^{-3} S·cm^{-1} and the sodium solid-state battery employing it can be operated at voltage up to 4.2 V against the cathode Na_xCoO_2, demonstrating its outstanding electrochemical stability;[18] however, the high sintering temperatures (>1000 °C), undesirable mechanical properties and significant grain boundary resistances are unfavorable for the practical application of oxide-based Na^+ conductors.[19] Rare-earth-containing halides have wide electrochemical windows and excellent electrochemical compatibility toward oxide cathode materials, as well as good mechanical deformability and scale-up capability, which is why they are viewed as promising candidates for catholyte materials.[20, 21] Nevertheless, recent instabilities against sulfide separators in their lithium counterparts,[22] suggest that chemical stability may remain an issue in Na^+-based halides as well.

These halides, when synthesized by conventional high temperature solid state reactions, often suffer from a low ionic conductivity.[20] For instance, Na_3InCl_6 crystallizing in space group $P\bar{3}1c$ was synthesized by the Bridgman furnace melting method, which only shows an ionic conductivity of ~10^{-9} S·cm^{-1} at room temperature.[23] In addition, calculation results also predict that the $C2m$ and $P3m1$ phases of Na_3InCl_6 can be experimentally synthesized.[24] In 2018, Asano *et al.* reported that a mechanochemically assisted synthesis protocol enables ionic conductivities

of Li_3YCl_6 and Li_3YBr_6 to reach as high as 0.5 and 1.7×10^{-3} S·cm^{-1} at room temperature, respectively.[25] Similarly, a higher conductivity has also been observed for ball milled sodium halide Na_2ZrCl_6 without subsequent heat treatment (up to 1.8×10^{-5} S·cm^{-1}) in comparison to the annealed counterpart (6.9×10^{-8} S·cm^{-1}).[26] In both cases the difference in ionic conductivity can be linked to the structure being affected by synthesis. High energy ball milling often leads to low crystallinity phases with significant amounts of point defects, stacking faults or even a difference in average symmetry that heal out or transform at elevated temperatures.[27-30] To further enhance ionic conductivity, the common-use strategy aliovalent cation substitution were applied to halide. This has been effectively investigated by Zr^{4+} substitution in Na_3MCl_6 (M = Y or Er). Here, $Na_{2.25}Zr_{0.75}Y_{0.25}Cl_6$ and $Na_{2.4}Zr_{0.6}Er_{0.4}Cl_6$ show ionic conductivities of 6.6×10^{-5} and 3.5×10^{-5} S·cm^{-1}, about three and four orders of magnitude higher than that of Na_3YCl_6 and Na_3ErCl_6 reepectively.[31, 32] Besides cation doping, anion substitution is also commonly explored to develop more conductive solid electrolytes, where especially halogen mixing seems beneficial for the conductivity.[33, 34] For example, the incorporation of chlorine in Li_2ZrF_6 enhances its room temperature ionic conductivity by about five orders of magnitude up to 5.5×10^{-7} S·cm^{-1} in Li_2ZrF_5Cl because of weaker Li-Cl bonds enabling more facile Li-ion transfer.[35] Additionally, for a series of compounds $Li_3YBr_xCl_{6-x}$ synthesized by co-melting of the precursors, the composition $Li_3YCl_{4.5}Br_{1.5}$ (x=1.5) crystallizes in trigonal $P\bar{3}m1$ phase (like Li_3YCl_6), while the compositions $Li_3YCl_{6-x}Br_x$ with x = 3, 4.5 crystallizes in monoclinic $C2/m$ phase (like Li_3YBr_6) and the halogen mixing allows higher conductivities (maximum of 5.4×10^{-3} S·cm^{1} at 30 °C for $Li_3YBr_{4.5}Cl_{1.5}$) especially when compared to that of Li_3YCl_6 (4.9×10^{-5} S·cm^{-1} at 30 °C).[36] Similarly, $Li_3InBr_xCl_{6-x}$ series compounds synthesized by ball milling and subsequent annealing also show various ionic conductivities, which reach a maximum of 1.2×10^{-4} S·cm^{1} at x = 3.[37] A similar complex relationship between composition and structure was also observed in halogen-mixed sodium solid solution $Na_3GdBr_xI_{6-x}$ system. Investigations on single crystals and powder samples revealed that the cryolite-type $P2_1/n$ structure occurs for x < 1. For x > 3, a new $Na_3GdBr_xI_{6-x}$ type appears (monoclinic, $C2/m$). In between, it adopts a monoclinic $C2/c$ phase. And the impedance measurements show a gradual decrease of the activation energy with increasing iodide content in the region with the unchanged crystal structure.[38] Here, a complex synergy of a softer lattice, change in average structure and thereby migration pathway, bottleneck expansion but also configuration entropy are deemed possible reasons. Beyond that it allows an additional degree of freedom in the design of halide solid electrolytes.

Motivated by the significant ionic conductivity enhancement of anion doped lithium halides, a series of anion mixed solid solutions of $Na_3InCl_{6-x}Br_x$ ($0 \leq x \leq 2$) is successfully synthesized by a mechanochemically assisted method. By using X-ray diffraction analyses, this work shows that a ball-milled $Na_3InCl_{6-x}Br_x$ solid solution series crystallizes in the monoclinic $P2_1/n$ space group, while upon subsequent annealing the solid solutions transform into the known trigonal phase in space group $P\bar{3}1c$ which shows a greater anion solubility. In $Na_3InCl_{6-x}Br_x$ only slight improvements to the ionic conductivity are observed possibly due to an unfavorable trade-off between high pre-factor and low activation energy resulting from an enthalpy-entropy compensation behavior fulfilling the Meyer-Neldel rule. This work extends the concept of synthesis-controlled polymorphism of the anion mixing of solid solutions based on rare-earth-containing sodium halides and reveals a limited transport performance improvement of sodium halide upon anion substitution.

Methods

Synthesis. All synthesis work was performed under an inert Argon or vacuum atmosphere. For the mechanochemical synthesis, stoichiometric amounts of NaCl (Merck, 99.5%, pre-dried at 200 °C for 48 h under dynamic vacuum), $InCl_3$ (Merck, 99.99%), and NaBr (Alfa Aesar, 99.99%) were put into ball mill cups. The mass ratio between milling media (ZrO_2, 5 mm diameter) and precursors was 30:1. The planetary ball milling was carried out by the Fritsch Pulverisette 7 at 100 rpm and 300 rpm for 10 minutes respectively to initially mix the precursors uniformly. And then the ball-milling was performed for 99 cycles in reverse mode, with one cycle consisting of milling at 500 rpm for 15 minutes and rest for 5 minutes to allow for cooling. Afterwards, the ball-milled powders were pelletized by a custom-made manual screw press and transferred into a quartz ampoule which was pre-dried at 800 °C under a dynamic vacuum for 2 hours. These ampoules were sealed under a vacuum and placed in a preheated tube-furnace. After annealing at 200 °C for 2 hours, the pellets were cooled by air quenching to ensure precise heating time and subsequently hand-ground into powders for further characterization.

X-ray diffraction for Rietveld. All samples were sealed in 0.5 mm-diameter glass capillaries for X-ray diffraction measurements because of their air sensitivity. Due to the relatively lower crystallinity of ball milled samples, X-ray diffraction measurements on them were performed with a STOE STADI P diffractometer (Ag $K_{\alpha 1}$ radiation, $\lambda = 0.5594$ Å; curved Ge(111)

monochromator, four Mythen K detector) with more higher resolution detectors in Debye-Scherrer scan mode at room temperature. Data collection was carried out for every sample in 0.015° steps. X-ray diffraction experiments of subsequently annealed samples were performed with a STOE STADI P diffractometer (Mo $K_{\alpha 1}$ radiation, $\lambda = 0.7093$ Å; curved Ge(111) monochromator, two Mythen 2K detectors) in Debye-Scherrer scan mode at room temperature. Data collection was carried out for every sample in 0.015° steps.

Rietveld analysis. The Rietveld refinement against X-ray diffraction data was performed with the TOPAS Academic software package.[39, 40] Rietveld refinements include (1) background of the Chebychev polynomial function, (2) scaling factor, (3) lattice parameters, (4) peak shape parameters from the modified Thompson-Cox-Hastings pseudo-Voigt function, (5) site fractional coordinates and occupancy factors, and the (6) isotropic displacement parameters. At last, all parameters were allowed to refine simultaneously to ensure stability of the parameters of the best possible refinement. The quality of the refinements was estimated by the indicators R_{wp} and goodness-of-fit (GoF).[41] All applied constraints and refined structural information can be found tabulated in the Supporting Information.

Amorphous content estimation. LaB_6 was used as a reference material due to its common use as a standard material for X-ray diffraction and the reason that its Bragg reflection at ~1.51 $Å^{-1}$ does not overlap with reflections of the ball milled samples.[42] The ball milled sample together with LaB_6 (Alfa-Aesar, 99.5%) were weighed (mass ratio 4:1) first, so the weights of the crystalline phase of the ball milled sample (w_c), the amorphous phase of the ball milled sample (w_a) and LaB_6 (w_{LB}) follow the equation:

$$(w_c+w_a):w_{LB} = 4:1 \tag{1}$$

Then the chemicals were mixed uniformly using an agate mortar and sealed in 0.5 mm diameter glass capillaries for X-ray diffraction measurements performed as described above (Mo $K_{\alpha 1}$ radiation, $\lambda = 0.7093$ Å; curved Ge(111) monochromator, Mythen 2K detector). A Rietveld refinement estimates crystalline material content and allows to determine the weight ratio between the crystalline phase of the ball milled sample and LaB_6 (r_{wt}) which is supposed to equal w_c:w_{LB}. Hence the amorphous phase content (c_a) can be evaluated:

$$c_a = \frac{4 - r_{wt}}{4} \tag{2}$$

Electrochemical Impedance Spectroscopy. Ionic conductivities, activation energies and

prefactors were extracted from temperature dependent electrochemical impedance spectroscopy. Approximately 150 mg of each sample were preliminarily pelletized by a custom-made manual screw press and then isostatically pressed under 330 MPa for 40 min. Subsequently, the pellets were coated with thin gold electrodes using sputter deposition and then enclosed in pouch cells contacted by aluminum tabs. The impedance was measured with an SP-300 impedance analyzer (Biologic SAS, EC-Lab) applying excitation voltages with an amplitude of 10 mV and frequencies in the range of 7 MHz to 100 mHz from -40 to 60 °C. The spectra at low temperature were too resistive to be resolved and were therefore excluded. And then the spectra were analyzed by RelaxIS 3 (rhd instruments). To only fit reliable data (less than 2% relative residuals in the Kramers-Kronig test for linearity), the ultrahigh and ultralow frequency ranges were restricted during analyses.

Results and discussions

Structural analyses. The collected powder X-ray diffraction patterns of ball milled $Na_3InCl_{6-x}Br_x$ ($0 \leq x \leq 2$) are shown in ***Figure 1a***. The similarity of X-ray diffraction patterns reveals that the structure of the Br-substituted compounds resembles that of ball milled Na_3InCl_6, except for additional reflections marked with asterisks (*) in the pattern of the nominal composition $Na_3InCl_4Br_2$. Additionally, shifts in the reflection positions to smaller *q*-values upon bromine substitution indicate an enlargement of the unit cell. However, the X-ray diffraction pattern of the purely ball milled Na_3InCl_6 does not match that expected from the structure of Na_3InCl_6 synthesized by the Bridgman furnace melting method reported previously.[23] This implies a different, yet undescribed phase of Na_3InCl_6 adopted when prepared by ball milling. The X-ray diffraction pattern resemblance with similar compositions (Na_3ErCl_6 and Na_3YCl_6) crystalizing in the cryolite-type $P2_1/n$ space group as previously observed allows the assumption that Na_3InCl_6 adopts the cryolite-like structure as well.[31, 32]

Nevertheless, in order to confirm that a $P2_1/n$ structure-type $Na_3InCl_{6-x}Br_x$ series forms with ball milling, Rietveld refinements were employed to determine the structure of exclusively ball milled samples. However, a possible amorphous phase contents of ball milled $Na_3InCl_{6-x}Br_x$ may lead to inaccurately refined crystal information (based on wrong assumptions e.g. stoichiometry), hence they were estimated (see Methods section) except for the $Na_3InCl_4Br_2$ sample, due to the overlapping between its additional reflections and LaB_6 reflections (***Figure S1a***). The refined results

show that the weight ratio between the crystalline phase of the ball milled sample and LaB_6 is close to the initially weighed in ratio of 4:1 (***Figure S1g***), indicating that the ball milled $Na_3InCl_{6-x}Br_x$ contains no significant amount of amorphous phase. This means ball milled compounds in the $Na_3InCl_{6-x}Br_x$ ($0 \leq x \leq 2$) series of compounds are mainly crystalline allowing Rietveld refinements to identify the average crystal structure.

Rietveld refinements (***Figure S2*** *and* ***Tables S2-6***) show that the $Na_3InCl_{6-x}Br_x$ ($0 \leq x \leq 1.5$) crystalize in the $P2_1/n$ cryolite-type phase, while the nominal $Na_3InCl_4Br_2$ contains a side phase (~20.0(5) wt.%) indexed in space group $P2_12_12_1$ analogous to $NaInBr_4$,[43] as observed in the diffraction pattern. ***Figure 1b*** displays the structure of the ball milled $Na_3InCl_{6-x}Br_x$ exemplarily for Na_3InCl_5Br which consists of two In^{3+} ions (Wyckoff 2*a*), six Na^+ ions (Wyckoff 4*e* and 2*d*), and twelve Cl^-/Br^- ions (Wyckoff 4*e*) per unit cell (formula units per unit cell $Z = 2$). In^{3+} ions are octahedrally coordinated by halogen anions at the corner and center of the unit cell. $NaCl_{6-x}Br_x^{5-}$ prisms consist of Na^+ ion at the Wyckoff 4*e* positions and six coordinated halogen ions. While $NaCl_{6-x}Br_x^{5-}$ octahedra are located at the edges along *a*-axis and center of *bc*-planes of the unit cell, with Na^+ at the Wyckoff 2*d* position and Cl^-/Br^- at three separate Wyckoff 4*e* positions. $NaCl_{6-x}Br_x^{5-}$ prisms share corners or edges with $NaCl_{6-x}Br_x^{5-}$ octahedra and $InCl_{6-x}Br_x^{3-}$ octahedra. While $NaCl_{6-x}Br_x^{5-}$ octahedra and $InCl_{6-x}Br_x^{3-}$ octahedra are corner-sharing.

Previous reports show that subsequent heat treatment has a significant impact on the structure and transport properties of mechanically synthesized halide solid electrolyte.[26, 28, 29] To investigate the influence of subsequent heat treatment on the ball milled $Na_3InCl_{6-x}Br_x$ series, the compounds were annealed at 200 °C for 2 hours. A preliminary X-ray diffraction pattern comparison with literature shows that the annealed $Na_3InCl_{6-x}Br_x$ compounds transform into a trigonal phase in space group $P\bar{3}1c$ which resembles the structure of Na_3InCl_6 synthesized by the Bridgman furnace melting method (***Figure 1c***).[23] Then Rietveld refinements against X-ray diffraction data were carried out to identify the phase purity and structural details of the annealed $Na_3InCl_{6-x}Br_x$ series using the reported trigonal structure of Na_3InCl_6 as starting model. Thereby, a previously identified sodium ion disorder in Na_3InCl_6 at elevated temperatures (450 K) with an additional sodium site (Wyckoff 2*c*, occupancy of ~7%) octahedrally coordinated by Cl^- was tested in the refinements.[23] As the refinement results statistics suggested no obvious difference between using the disordered and ordered structure-type model (***Figure S3***) and the refined sodium occupancy at Wyckoff 4*f* site is over 100% using the disordered model (previously reported ~97%) implying

an overfitting (***Table S16***),[23] the proposed disordered structure was disregarded and the more commonly adopted ordered Na_3InCl_6 structure was used as starting model to refine the annealed Br-substituted samples.

The refinement results suggest that the annealed $Na_3InCl_{6-x}Br_x$ ($0 \leq x \leq 1.5$) phases crystalize in the pure trigonal polymorph and the content of the side phase indexed in space group $P2_12_12_1$ in nominal $Na_3InCl_4Br_2$ reduces to ~3.2(4) wt.% which is much lower than contained within the ball milled sample and may speculatively be attributed to a further reaction of residual Na*X* and the possibly NaInX_4 (*X* = Cl or Br) side phase into the main phase under high temperature. A similar phase transition is also observed in the cation substituted $Na_{2+x}Zr_{1-x}In_xCl_6$ series, which tends to partially transform from the monoclinic $P2_1/n$ phase into the trigonal $P\bar{3}1c$ phase under higher annealing temperature as well.[44] As shown in ***Figure 1d,*** the unit cell of the ordered $P\bar{3}1c$ polymorph adopted by the annealed $Na_3InCl_{6-x}Br_x$ exemplarily represented by Na_3InCl_5Br is composed of two In^{3+} ions (Wyckoff 2*d*), six Na^+ ions (Wyckoff 4*f* and 2*a*), and twelve Cl^-/Br^- ions (Wyckoff 12*i*) with formula units per unit cell $Z = 2$. Unlike the $P2_1/n$ phase, all cations of $Na_3InCl_{6-x}Br_x$ in the space group of $P\bar{3}1c$ are octahedrally coordinated by halide anions. $NaCl_{6-x}Br_x^{5-}$ octahedra (Na^+ at Wyckoff 2*a* site) are located at the edges along the *c*-axis of the unit cell which share corners with the other $NaCl_{6-x}Br_x^{5-}$ octahedra (Na^+ at Wyckoff 4*f* site) and share edges with $InCl_{6-x}Br_x^{3-}$ octahedra, while $NaCl_{6-x}Br_x^{5-}$ octahedra (Na^+ at Wyckoff 4*f* site) and $InCl_{6-x}Br_x^{3-}$ octahedra are connected by a trigonal face.

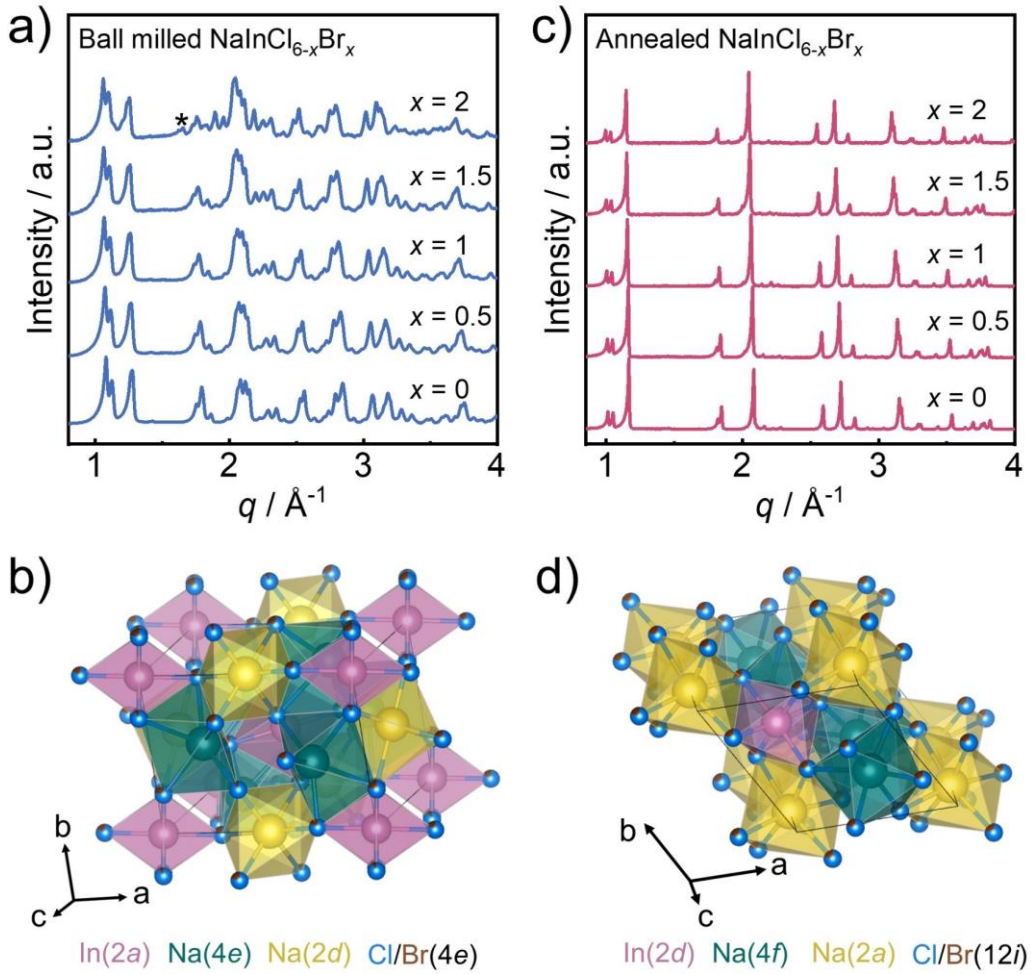

Figure 1. a) *X-ray diffraction patterns and* ***b)*** *crystal structure represented by Na_3InCl_5Br of the ball milled $Na_3InCl_{6-x}Br_x$ ($0 \leq x \leq 2$) series.* ***c)*** *X-ray diffraction patterns and* ***d)*** *crystal structure represented by Na_3InCl_5Br of the subsequently annealed $Na_3InCl_{6-x}Br_x$ ($0 \leq x \leq 2$) series.*

Previous calculation results show that the structure of the sodium halides Na_3MX_6 strongly depends on the type and size of metal cation *M* and halide anion *X*.[45] However, the refinement results demonstrate that the synthesis condition also significantly impacts the structure of sodium halide, even its anion solubility. Moreover, it can be speculated that the $P\bar{3}1c$ phase of Na_3InBr_6 (theoretically proposed) is less stable than the competing phases of $NaInBr_4$ and NaBr under the current synthesis condition,[45] because of the presence of the $NaInBr_4$-type side phase.

Structure evolution of the $Na_3InCl_{6-x}Br_x$ solid solutions. To better understand the influence of synthesis protocol and bromine substitution on the structure of the $Na_3InCl_{6-x}Br_x$ series, the structural evolution of $Na_3InCl_{6-x}Br_x$ as obtained from Rietveld refinements is investigated.

Milled samples, monoclinic polymorph - ***Figure 2a*** displays that the refined Br^- fraction fits well

with the nominal content of the ball milled $Na_3InCl_{6-x}Br_x$ series ($0 \leq x \leq 1.5$) which corroborates the existence of anion mixed solid solution. Meanwhile the refined Br^- content of the nominal $Na_3InCl_4Br_2$ suggests off-stoichiometry in agreement with the notable side phase content. Because the six-fold coordinated Br^- radius (196 pm) is larger than that of Cl^- (181 pm),[46] the lattice parameters *a*, *b* and *c* as well as unit cell volume of ball milled $Na_3InCl_{6-x}Br_x$ expand linearly upon increased Br contents, in line with Vegard's law.[47] Meanwhile the β lattice parameter decreases linearly with substitution degree *x* (***Figure 2b-d***) which was also found to be similarly influenced by the aliovalent cation substitution in halides (Zr^{4+} doped Na_3ErCl_6 and Li_3InCl_6).[31, 48] The refined lattice parameters of $P2_1/n$ phase of the nominal $Na_3InCl_4Br_2$ are comparable with those of nominal $Na_3InCl_{4.5}Br_{1.5}$ as shown in ***Figure S4a-c***, consistent with the refined Br^- content, which further indicates the reliability of the refinement results of the ball milled samples. With increasing Br^- content, both the $InCl_{6-x}Br_x^{3-}$ octahedra and $NaCl_{6-x}Br_x^{5-}$ (Na^+ at Wyckoff 2*d* and 4*e* sites) polyhedra increase in volume as shown in ***Figure 2e-f***, which can be attributed to the average coordinated anion radius increase and potentially an effective cation-anion interaction weakening. Moreover, the $NaCl_{6-x}Br_x^{5-}$ prism is smaller than the $NaCl_{6-x}Br_x^{5-}$ octahedron at the same substitution degree *x*.

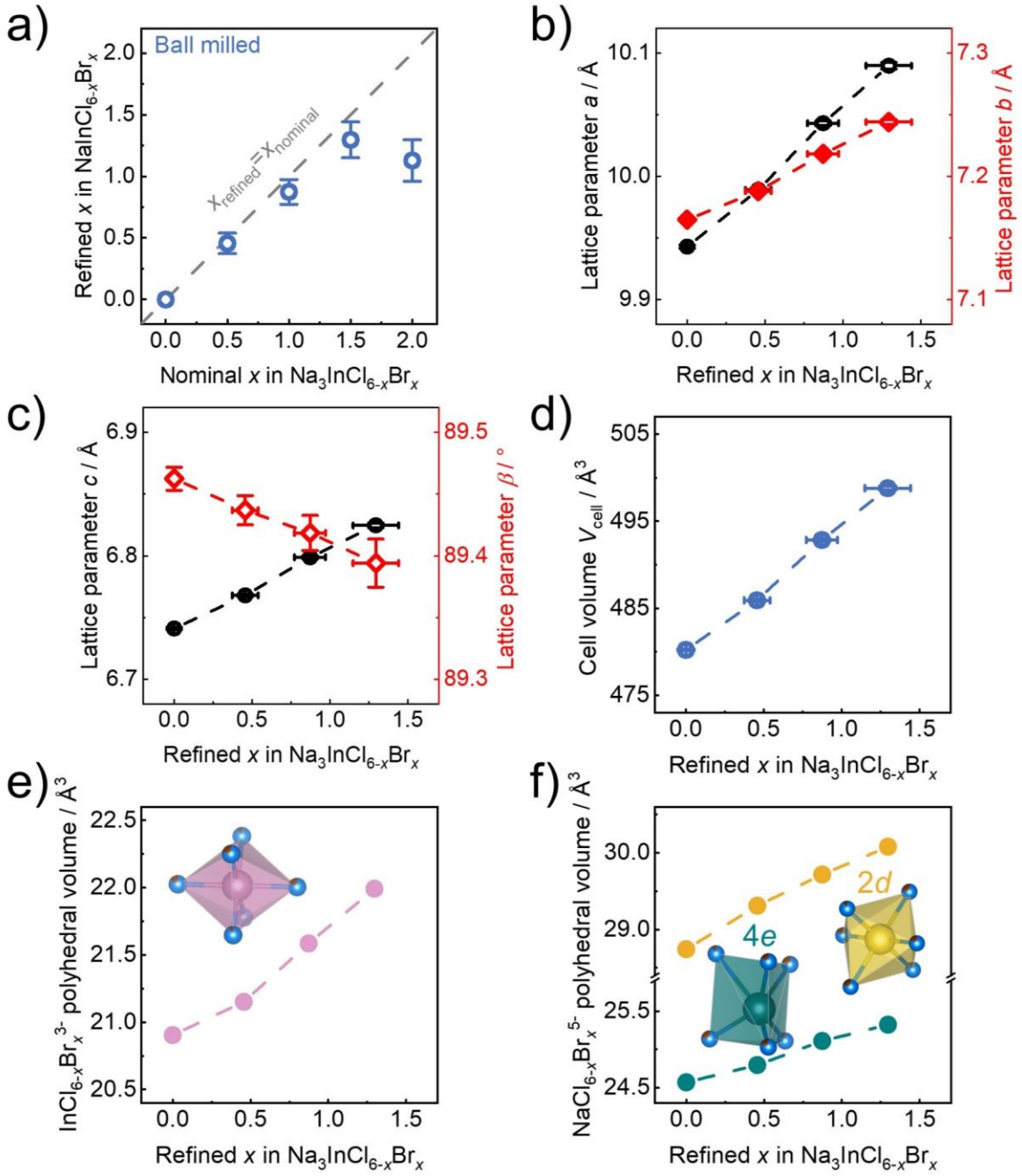

Figure 2. a) *Refined Br^- content against nominal Br^- content of the ball milled $Na_3InCl_{6-x}Br_x$.* ***b)*** *Lattice parameters a and b,* ***c)*** *lattice parameters c and β angle,* ***d)*** *unit cell volume V_{cell},* ***e)*** *$InCl_{6-x}Br_x^{3-}$ and* ***f)*** *$NaCl_{6-x}Br_x^{5-}$ polyhedral volume of the ball milled $Na_3InCl_{6-x}Br_x$ against the refined Br^- content. The uncertainties shown correspond to 3σ. The refined structure details of the nominal $Na_3InCl_4Br_2$ remain disregarded here since it suggests off-stoichiometry and a notable side phase content.*

Annealed samples, trigonal polymorph - An approximately linear behavior can be observed for the refined Br^- fraction as a function of the nominal content for the annealed $Na_3InCl_{6-x}Br_x$ series ($0 \leq x \leq 2$), demonstrating that the ball milled compounds transform into solid solutions with the trigonal structural polymorph excluding decomposition or side phase segregation upon annealing (***Figure 3a***). It is notable that the refined Br^- fraction of annealed $Na_3InCl_4Br_2$ is on-stoichiometric, combined with the significantly reduced amount of $NaInX_4$-type side phase, which indicates increased bromine solubility in the annealed $Na_3InCl_{6-x}Br_x$ solid solutions. Whether this is due to (1) the difference in structure-type, (2) increasing solubility at annealing temperature and then kinetically stabilized by air quenching or (3) non-sufficient reaction energy input from ball milling is unclear. The lattice parameters as well as unit cell and polyhedral volumes of the annealed $Na_3InCl_{6-x}Br_x$ series display a similar case with those of ball milled series, which approximately linearly expand upon increased Br^- content. The annealed $Na_3InCl_4Br_2$ also conforms to the linear behavior corroborating the reliability of the refined Br^- fraction and the existence of the $P\bar{3}1c$ phase $Na_3InCl_4Br_2$ solid solution. Moreover, unlike the monoclinic $P2_1/n$ phase, both the sodium sites with multiplicity of two and four are octahedrally coordinated by anion ions in the trigonal $P\bar{3}1c$ phase, so that their polyhedral volume has no significant difference (***Figure 3f***).

A direct comparison shows that the volume of octahedra with four-multiplicity sodium (Na^+ at Wyckoff 4*f* site) of the $P\bar{3}1c$ phase (~29 to 30 $Å^3$) is larger than that of the prism (Na^+ at Wyckoff 4*e* site) in the $P2_1/n$ phase (~24.5 to 25.5 $Å^3$), which leads to larger normalized unit cell volumes of annealed $Na_3InCl_{6-x}Br_x$ series compared to that of ball milled $Na_3InCl_{6-x}Br_x$ series with the same substitution degree *x* (***Figure S4d***).

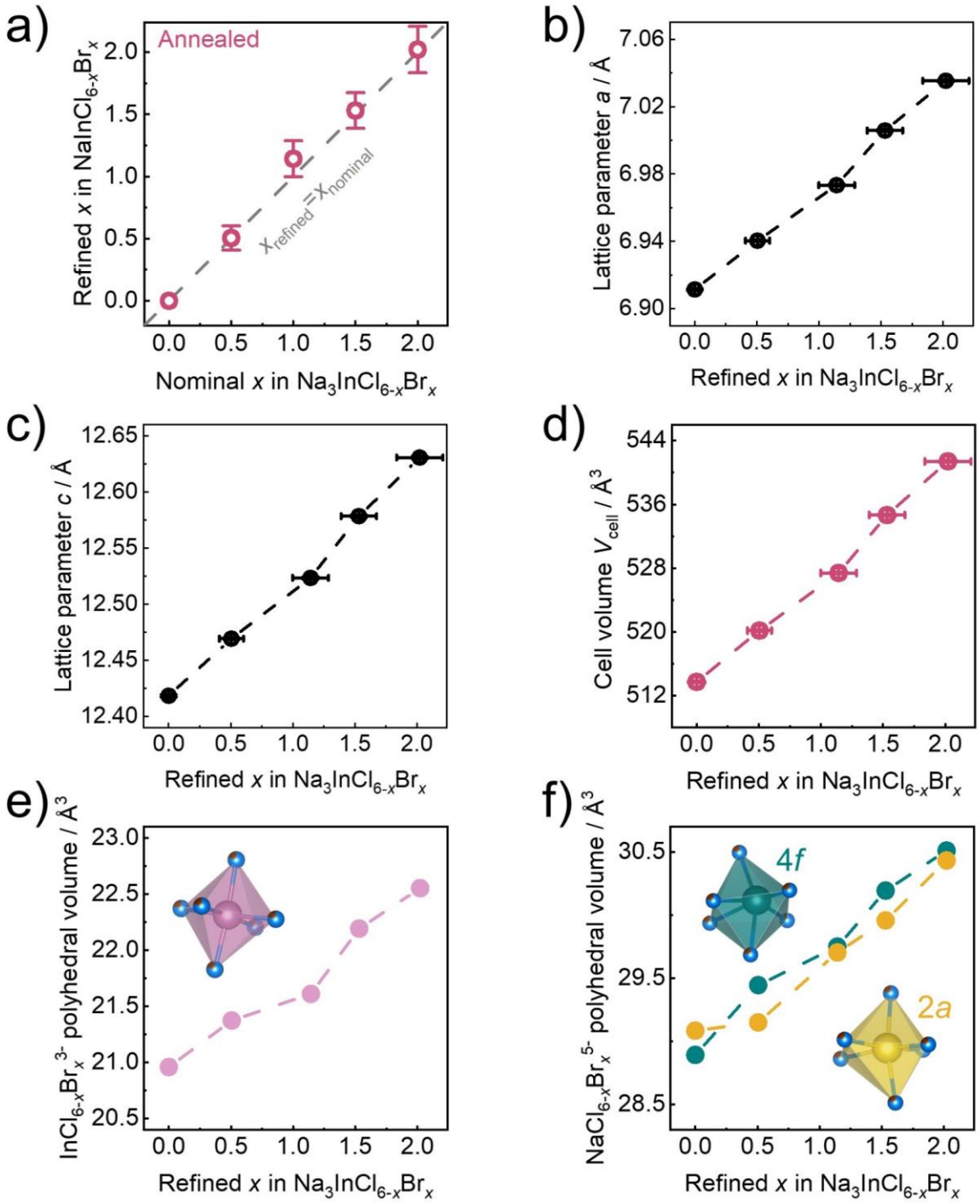

Figure 3. a) *Refined Br^- content against nominal Br^- content of the subsequently annealed $Na_3InCl_{6-x}Br_x$.* ***b)*** *Lattice parameters a,* ***c)*** *lattice parameters c,* ***d)*** *unit cell volume V_{cell},* ***e)*** *$InCl_{6-x}Br_x^{3-}$ and* ***f)*** *$NaCl_{6-x}Br_x^{5-}$ polyhedral volume of the subsequently annealed $Na_3InCl_{6-x}Br_x$ against the refined Br^- content. The uncertainties shown correspond to 3σ.*

Ionic transport properties. The Na^+ ion transport of the $Na_3InCl_{6-x}Br_x$ solid solution series synthesized by different procedures is evaluated using temperature-dependent electrochemical impedance spectroscopy. The impedance spectra measured at 60 °C and room temperature (25 °C) are displayed in ***Figures S5 and S6*** in Nyquist representation. All collected impedance spectra can be fitted with one equivalent circuit model (the inset of ***Figure S5a and S6a***) consisting of a parallel combination of resistor and constant phase element (CPE), in series with another CPE representing the blocking electrodes. The resolved impedance spectra exhibit a CPE α-values of ~0.95 and the capacitances of ~5×10^{-11} F can be associated to the process which is likely dominated by bulk transport. Nevertheless, the contributions of grain bulk and grain boundary cannot be deconvoluted and grain boundary contributions cannot be excluded,[49] thus derived values represent the total ionic conductivities. The Na^+ conductivities of $Na_3InCl_{6-x}Br_x$ solid solution synthesized by different procedures show linear Arrhenius behavior in the measured temperature ranges (see ***Figures 4a, b***). Here, nominal $Na_3InCl_4Br_2$ synthesized by ball milling remains disregarded due to large side phase contents. The obtained room-temperature conductivities (σ_{RT}) are shown in ***Figures 4c,*** as a function of the refined Br content. Even though the structure of $Na_3InCl_{6-x}Br_x$ changes continuously, its ionic conductivity does not show a continuous change, neither for ball milled solid solutions nor subsequently annealed solid solutions. One may speculate that this may be due to the sodium transport behavior of $Na_3InCl_{6-x}Br_x$ compounds is not exclusively being dominated by crystal geometry and the other structural descriptors (the local environment of Na^+, Br^-/Cl^- mixing uniformity, etc.), all of which can also have a significant impact on ionic conductivity.[50] Moreover, unlike the case of Br substituted doped Li_3InCl_6,[36] bromine substitution can only slightly improve the ionic conductivity within the $Na_3InCl_{6-x}Br_x$ series. Previous calculation results suggest that $Li_3InCl_3Br_3$ separates into Br-rich and Cl-rich regions and this kind of separation increases Li ion diffusivity at the interface.[50] Here, one may assume that due to the limited Br solubility of the $Na_3InCl_{6-x}Br_x$ series, the series cannot form the Br-rich region in the Br-doped $Na_3InCl_{6-x}Br_x$ crystal so that its ionic conductivity does not increase dramatically in comparison to pristine Na_3InCl_6. The ball milled solid solutions do not exhibit an overwhelmingly superior transport performance compared with annealed samples, as previously observed in other rare-earth-containing chloride-type sodium ionic conductors and it may be attributed to the lack of significant amorphous phase which has been shown beneficial for Na^+ movement.[26, 32] Here, both synthesis procedures result in crystalline phases, forming in different polymorphs with similar ionic conductivities. The activation energies (E_a) and Arrhenius

prefactors (σ_0) were extracted from the linear Arrhenius fitting. Here, the incorporation of Br results in an initial increase of activation energy (***Figure 4d***) in both structural polymorphs, where upon further Br substitution the activation energies slightly reduce (ball milled) or stagnate (annealed). Meanwhile prefactor σ_0 of the Br doped compounds is also greater than pristine Na_3InCl_6 for both ball milled and subsequently annealed series as shown in ***Figure S7b***. As both the enthalpy and entropy of carrier migration are convoluted in the activation barrier and Arrhenius prefactor,[51] the ionic conductivities of the Br doped compounds are significantly impacted by the synergistic effect of E_a and σ_0. Meyer-Neldel rule is widely observed for semiconductors and ionic conductors, which points out a linear behavior between the natural logarithm of prefactor σ_0 ($\ln(\sigma_0)$) and activation energy E_a.[52, 53] As shown in ***Figure S7c***, the $\ln(\sigma_0)$ of $Na_3InCl_{6-x}Br_x$ as a function of E_a is linear for both ball milled and subsequently annealed series, indicating both the $P\bar{3}1c$ and $P2_1/n$ phase $Na_3InCl_{6-x}Br_x$ solid solutions follow the Meyer-Neldel rule. Nevertheless, the observed Meyer-Neldel rule behavior of $Na_3InCl_{6-x}Br_x$ implies an unfavorable trade-off between high prefactor and low activation energy hindering the Br doped compounds to achieve high ionic conductivity.

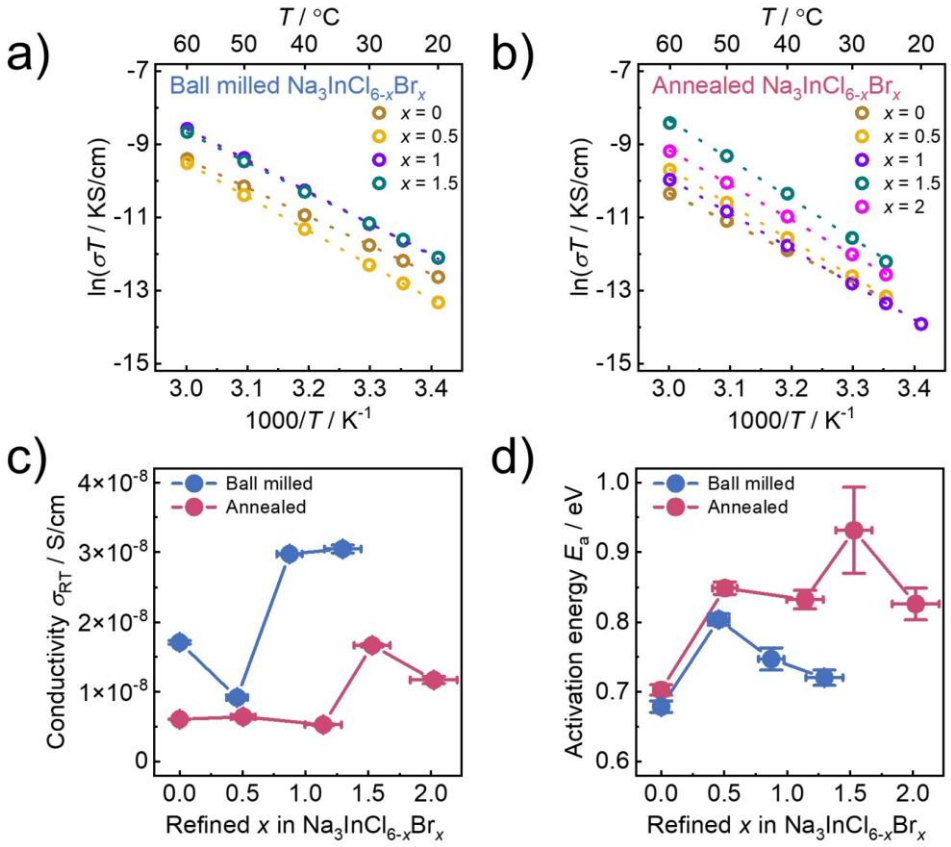

Figure 4. *Arrhenius plots from the temperature dependent impedance of* ***a)*** *ball milled and* ***b)*** *subsequently annealed $Na_3InCl_{6-x}Br_x$. The spectra of some samples at low temperature are too resistive to be resolved and are therefore excluded from the Arrhenius plot.* ***c)*** *Ionic conductivities of $Na_3InCl_{6-x}Br_x$ measured at room temperature (25 °C).* ***d)*** *Activation energies of $Na_3InCl_{6-x}Br_x$. The uncertainties shown correspond to 3σ.*

Overall the complex ionic transport behavior cannot be fully described but can be contextualized with previously observed principles; i) a trend towards larger ionic conductivities in the monoclinic polymorph is in line with previous observations in other sodium metal halides likely originating from a more favorable diffusion pathway.[54] Any beneficial contribution from a large amount of amorphous side phase can be excluded here.[26, 28] ii) Stoichiometric sodium metal halides without intrinsically stabilized sodium point defects (vacancies) generally from aliovalent cation substitution exhibit rather low ionic conductivities at room temperature.[31, 32] iii) Local environment change of the sodium ions (e.g. bonds between Na^+ and coordinated anion *X*, polyhedral expansion) cannot exclusively dominate the transport performance of the sodium-based halides. As this strategy seems to work for lithium-based halides,[35] it may imply that the strategies to tune ion transport in lithium-based halides may not be as effective in the sodium-analogues.

Conclusion

In this work, we successfully synthesized a series of anion mixed solid solutions $Na_3InCl_{6-x}Br_x$ ($0 \leq x \leq 2$) by ball milling and subsequently annealing. By using X-ray diffraction, we can show that the ball milling as-prepared $Na_3InCl_{6-x}Br_x$ solid solution series crystallizes in a monoclinic polymorph (space group $P2_1/n$) of the cryolite structure-type, while subsequent annealing transforms this solid solution series into the commonly observed trigonal polymorph (space group $P\bar{3}1c$) with a larger anion solubility. In both polymorphs the Br^- substitution leads to an expansion of the unit cell with approximately linear increases in polyhedral volumes. However, the activation energy increases upon bromine substitution which therefore can only slightly improve the ionic conductivity in the $Na_3InCl_{6-x}Br_x$ compounds. This work further highlights the complex synthesis-structure relationship within sodium metal halides even upon halogen-mixing and their

limited anion solubility. It further shows a more limited transport performance improvement of these sodium-metal halides upon halide anion substitution in comparison to the lithium analogues such as $Li_3YCl_{6-x}Br_x$ and $Li_3InCl_{6-x}Br_x$.

Acknowledgments

This work is funded by the Ministry of Culture and Science of the State North Rhine Westphalia in course of the International Graduate School of Battery Chemistry, Characterization, Analysis, Recycling and Application (BACCARA). The authors acknowledge financial support within the NATTER funded by Bundesministerium für Bildung und Forschung (BMBF project 03XP0525B).

Supporting Information

The Supporting Information includes amorphous content evaluation results, Rietveld refinement results, structural evolution of ball milled $Na_3InCl_{6-x}Br_x$, the room-temperature and 60 °C evaluated impedance data, ionic conductivities of $Na_3InCl_{6-x}Br_x$ measured at 60 °C, prefactors of $Na_3InCl_{6-x}Br_x$, Meyer-Neldel rule behavior of $Na_3InCl_{6-x}Br_x$.

References

1. Yang, H.-L.; Zhang, B.-W.; Konstantinov, K.; Wang, Y.-X.; Liu, H.-K.; Dou, S.-X., Progress and Challenges for All‐Solid‐State Sodium Batteries. *Advanced Energy and Sustainability Research* **2021,** *2* (2).
2. Oh, J. A. S.; He, L.; Chua, B.; Zeng, K.; Lu, L., Inorganic sodium solid-state electrolyte and interface with sodium metal for room-temperature metal solid-state batteries. *Energy Storage Materials* **2021,** *34*, 28-44.
3. Nayak, P. K.; Yang, L.; Brehm, W.; Adelhelm, P., From Lithium-Ion to Sodium-Ion Batteries: Advantages, Challenges, and Surprises. *Angew. Chem. Int. Ed. Engl.* **2018,** *57* (1), 102-120.
4. Janek, J.; Zeier, W. G., Challenges in speeding up solid-state battery development. *Nature Energy* **2023,** *8* (3), 230-240.
5. Zheng, F.; Kotobuki, M.; Song, S.; Lai, M. O.; Lu, L., Review on solid electrolytes for all-solid-state lithium-ion batteries. *J. Power Sources* **2018,** *389*, 198-213.
6. Zhu, Z.; Chu, I.-H.; Deng, Z.; Ong, S. P., Role of Na+ Interstitials and Dopants in Enhancing the Na+ Conductivity of the Cubic Na3PS4 Superionic Conductor. *Chem. Mater.* **2015,** *27* (24), 8318-8325.
7. Nguyen, H.; Banerjee, A.; Wang, X.; Tan, D.; Wu, E. A.; Doux, J.-M.; Stephens, R.; Verbist, G.; Meng, Y. S., Single-step synthesis of highly conductive Na3PS4 solid electrolyte for sodium all solid-state batteries. *J. Power Sources* **2019,** *435*, 126623.
8. Nonemacher, J. F.; Naqash, S.; Tietz, F.; Malzbender, J., Micromechanical assessment of Al/Y-substituted NASICON solid electrolytes. *Ceram. Int.* **2019,** *45* (17, Part A), 21308-21314.
9. Go, W.; Kim, J.; Pyo, J.; Wolfenstine, J. B.; Kim, Y., Investigation on the Structure and Properties of Na3.1Zr1.55Si2.3P0.7O11 as a Solid Electrolyte and Its Application in a Seawater Battery. *ACS Applied Materials &*

Interfaces **2021,** *13* (44), 52727-52735.
10. Zhang, D.; Cao, X.; Xu, D.; Wang, N.; Yu, C.; Hu, W.; Yan, X.; Mi, J.; Wen, B.; Wang, L.; Zhang, L., Synthesis of cubic Na3SbS4 solid electrolyte with enhanced ion transport for all-solid-state sodium-ion batteries. *Electrochim. Acta* **2018,** *259*, 100-109.
11. Hayashi, A.; Noi, K.; Tanibata, N.; Nagao, M.; Tatsumisago, M., High sodium ion conductivity of glass–ceramic electrolytes with cubic Na3PS4. *J. Power Sources* **2014,** *258*, 420-423.
12. Krauskopf, T.; Muy, S.; Culver, S. P.; Ohno, S.; Delaire, O.; Shao-Horn, Y.; Zeier, W. G., Comparing the Descriptors for Investigating the Influence of Lattice Dynamics on Ionic Transport Using the Superionic Conductor Na3PS4–xSex. *J. Am. Chem. Soc.* **2018,** *140* (43), 14464-14473.
13. Chen, S.; Wu, C.; Shen, L.; Zhu, C.; Huang, Y.; Xi, K.; Maier, J.; Yu, Y., Challenges and Perspectives for NASICON-Type Electrode Materials for Advanced Sodium-Ion Batteries. *Adv. Mater.* **2017,** *29* (48), 1700431.
14. Park, H.; Kang, M.; Park, Y.-C.; Jung, K.; Kang, B., Improving ionic conductivity of Nasicon (Na3Zr2Si2PO12) at intermediate temperatures by modifying phase transition behavior. *J. Power Sources* **2018,** *399*, 329-336.
15. Rao, Y. B.; Bharathi, K. K.; Patro, L. N., Review on the synthesis and doping strategies in enhancing the Na ion conductivity of Na3Zr2Si2PO12 (NASICON) based solid electrolytes. *Solid State Ionics* **2021,** *366-367*, 115671.
16. Santhoshkumar, B.; Rao, P. L.; Ramanathan, K. V.; Bera, A. K.; Yusuf, S. M.; Hathwar, V. R.; Pahari, B., Structure and ionic conductivity of Na3+xSc2SixP3-xO12 (x=0.0, 0.2, 0.4, 0.8) NASICON materials: A combined neutron diffraction, MAS NMR and impedance study. *Solid State Sciences* **2021,** *111*, 106470.
17. Fuchs, T.; Culver, S. P.; Till, P.; Zeier, W. G., Defect-Mediated Conductivity Enhancements in Na3–xPn1–xWxS4 (Pn = P, Sb) Using Aliovalent Substitutions. *ACS Energy Letters* **2020,** *5* (1), 146-151.
18. Kehne, P.; Guhl, C.; Ma, Q.; Tietz, F.; Alff, L.; Hausbrand, R.; Komissinskiy, P., Sc-substituted Nasicon solid electrolyte for an all-solid-state NaxCoO2/Nasicon/Na sodium model battery with stable electrochemical performance. *J. Power Sources* **2019,** *409*, 86-93.
19. Anantharamulu, N.; Koteswara Rao, K.; Rambabu, G.; Vijaya Kumar, B.; Radha, V.; Vithal, M., A wide-ranging review on Nasicon type materials. *JMatS* **2011,** *46* (9), 2821-2837.
20. Li, X.; Liang, J.; Yang, X.; Adair, K. R.; Wang, C.; Zhao, F.; Sun, X., Progress and perspectives on halide lithium conductors for all-solid-state lithium batteries. *Energy & Environmental Science* **2020,** *13* (5), 1429-1461.
21. Kwak, H.; Wang, S.; Park, J.; Liu, Y.; Kim, K. T.; Choi, Y.; Mo, Y.; Jung, Y. S., Emerging Halide Superionic Conductors for All-Solid-State Batteries: Design, Synthesis, and Practical Applications. *ACS Energy Letters* **2022,** *7* (5), 1776-1805.
22. Rosenbach, C.; Walther, F.; Ruhl, J.; Hartmann, M.; Hendriks, T. A.; Ohno, S.; Janek, J.; Zeier, W. G., Visualizing the Chemical Incompatibility of Halide and Sulfide-Based Electrolytes in Solid-State Batteries. **2023,** *13* (6), 2203673.
23. Yamada, K.; Kumano, K.; Okuda, T., Conduction path of the sodium ion in Na3InCl6 studied by X-ray diffraction and 23Na and 115In NMR. *Solid State Ionics* **2005,** *176* (7), 823-829.
24. Lian, Y.; Wu, M.; Xu, B.; He, B.; Liu, G.; Shi, J.; Kuang, Q.; Wang, H.; Ouyang, C., Phase-structure design for sodium chloride solid electrolytes with outstanding performance: a first-principles approach. *Journal of Materials Chemistry A* **2023,** *11* (4), 1906-1919.
25. Asano, T.; Sakai, A.; Ouchi, S.; Sakaida, M.; Miyazaki, A.; Hasegawa, S., Solid Halide Electrolytes with High Lithium-Ion Conductivity for Application in 4 V Class Bulk-Type All-Solid-State Batteries. **2018,** *30* (44), 1803075.
26. Kwak, H.; Lyoo, J.; Park, J.; Han, Y.; Asakura, R.; Remhof, A.; Battaglia, C.; Kim, H.; Hong, S.-T.; Jung, Y. S., Na2ZrCl6 enabling highly stable 3 V all-solid-state Na-ion batteries. *Energy Storage Materials* **2021,** *37*, 47-54.
27. Sebti, E.; Evans, H. A.; Chen, H.; Richardson, P. M.; White, K. M.; Giovine, R.; Koirala, K. P.; Xu, Y.; Gonzalez-Correa, E.; Wang, C.; Brown, C. M.; Cheetham, A. K.; Canepa, P.; Clement, R. J., Stacking Faults Assist Lithium-Ion Conduction in a Halide-Based Superionic Conductor. *J Am Chem Soc* **2022,** *144* (13), 5795-5811.
28. Schlem, R.; Muy, S.; Prinz, N.; Banik, A.; Shao-Horn, Y.; Zobel, M.; Zeier, W. G., Mechanochemical Synthesis: A Tool to Tune Cation Site Disorder and Ionic Transport Properties of Li3MCl6 (M = Y, Er) Superionic Conductors. *Advanced Energy Materials* **2020,** *10* (6), 1903719.
29. Park, J.; Han, D.; Kwak, H.; Han, Y.; Choi, Y. J.; Nam, K.-W.; Jung, Y. S., Heat treatment protocol for modulating ionic conductivity via structural evolution of Li3-xYb1-xMxCl6 (M = Hf4+, Zr4+) new halide superionic conductors for all-solid-state batteries. *Chem. Eng. J.* **2021,** *425*.
30. Schlem, R.; Burmeister, C. F.; Michalowski, P.; Ohno, S.; Dewald, G. F.; Kwade, A.; Zeier, W. G., Energy Storage Materials for Solid-State Batteries: Design by Mechanochemistry. **2021,** *11* (30), 2101022.

31. Schlem, R.; Banik, A.; Eckardt, M.; Zobel, M.; Zeier, W. G., Na3–xEr1–xZrxCl6—A Halide-Based Fast Sodium-Ion Conductor with Vacancy-Driven Ionic Transport. *ACS Applied Energy Materials* **2020,** *3* (10), 10164-10173.
32. Wu, E. A.; Banerjee, S.; Tang, H.; Richardson, P. M.; Doux, J.-M.; Qi, J.; Zhu, Z.; Grenier, A.; Li, Y.; Zhao, E.; Deysher, G.; Sebti, E.; Nguyen, H.; Stephens, R.; Verbist, G.; Chapman, K. W.; Clément, R. J.; Banerjee, A.; Meng, Y. S.; Ong, S. P., A stable cathode-solid electrolyte composite for high-voltage, long-cycle-life solid-state sodium-ion batteries. *Nature Communications* **2021,** *12* (1), 1256.
33. Till, P.; Agne, M. T.; Kraft, M. A.; Courty, M.; Famprikis, T.; Ghidiu, M.; Krauskopf, T.; Masquelier, C.; Zeier, W. G., Two-Dimensional Substitution Series Na3P1–xSbxS4–ySey: Beyond Static Description of Structural Bottlenecks for Na+ Transport. *Chem. Mater.* **2022,** *34* (5), 2410-2421.
34. Zhang, X.; Phuah, K. C.; Adams, S., Anion Control of the Electrolyte Na3–xSbS4–xBrx Extends Cycle Life in Solid-State Sodium Batteries. *Chem. Mater.* **2021,** *33* (23), 9184-9193.
35. Umeshbabu, E.; Maddukuri, S.; Hu, Y.; Fichtner, M.; Munnangi, A. R., Influence of Chloride Ion Substitution on Lithium-Ion Conductivity and Electrochemical Stability in a Dual-Halogen Solid-State Electrolyte. *ACS Applied Materials & Interfaces* **2022,** *14* (22), 25448-25456.
36. van der Maas, E.; Zhao, W.; Cheng, Z.; Famprikis, T.; Thijs, M.; Parnell, S. R.; Ganapathy, S.; Wagemaker, M., Investigation of Structure, Ionic Conductivity, and Electrochemical Stability of Halogen Substitution in Solid-State Ion Conductor Li3YBrxCl6–x. *The Journal of Physical Chemistry C* **2023,** *127* (1), 125-132.
37. Tomita, Y.; Matsushita, H.; Kobayashi, K.; Maeda, Y.; Yamada, K., Substitution effect of ionic conductivity in lithium ion conductor, LI3INBR6−xCLx. *Solid State Ionics* **2008,** *179* (21), 867-870.
38. Bohnsack, A.; Meyer, G., Ternäre Halogenide vom Typ A3MX6. V. Synthese, Kristallstrukturen und Natrium-Ionenleitfähigkeit der ternären Iodide Na3MI6 (M = Sm, Gd–Dy) sowie der Mischkristalle Na3GdBr6-xIx. **1997,** *623* (1-6), 837-843.
39. Rietveld, H. M., The Rietveld method. *Phys. Scr.* **2014,** *89* (9), 098002.
40. Coelho, A. A., TOPAS and TOPAS-Academic: an optimization program integrating computer algebra and crystallographic objects written in C++. *J. Appl. Crystallogr.* **2018,** *51* (1), 210-218.
41. Young, R. A., The Rietveld Method. *Oxford University Press: New York* **1993**.
42. Grazulis, S.; Chateigner, D.; Downs, R. T.; Yokochi, A. F. T.; Quiros, M.; Lutterotti, L.; Manakova, E.; Butkus, J.; Moeck, P.; Le Bail, A., Crystallography Open Database - an open-access collection of crystal structures. *J. Appl. Crystallogr.* **2009,** *42* (4), 726-729.
43. Staffel, T.; Meyer, G., Synthese und Kristallstrukturen von NalnBr4 und NaInI4. *Z. Anorg. Allg. Chem.* **1989,** *574* (1), 107-113.
44. Zhao, T.; Sobolev, A. N.; Schlem, R.; Helm, B.; Kraft, M. A.; Zeier, W. G., Synthesis-Controlled Cation Solubility in Solid Sodium Ion Conductors Na2+xZr1–xInxCl6. *ACS Applied Energy Materials* **2023,** *6* (8), 4334-4341.
45. Yu, S.; Kim, K.; Wood, B. C.; Jung, H.-G.; Chung, K. Y., Structural design strategies for superionic sodium halide solid electrolytes. *Journal of Materials Chemistry A* **2022,** *10* (45), 24301-24309.
46. Shannon, R., Revised effective ionic radii and systematic studies of interatomic distances in halides and chalcogenides. *AcCrA* **1976,** *32* (5), 751-767.
47. Denton, A. R.; Ashcroft, N. W., Vegard's law. *Phys. Rev. A* **1991,** *43* (6), 3161-3164.
48. Helm, B.; Schlem, R.; Wankmiller, B.; Banik, A.; Gautam, A.; Ruhl, J.; Li, C.; Hansen, M. R.; Zeier, W. G., Exploring Aliovalent Substitutions in the Lithium Halide Superionic Conductor Li3 – xIn1 – xZrxCl6 ($0 \leqslant x \leqslant 0.5$). *Chem. Mater.* **2021,** *33* (12), 4773-4782.
49. Irvine, J. T. S.; Sinclair, D. C.; West, A. R., Electroceramics: Characterization by Impedance Spectroscopy. **1990,** *2* (3), 132-138.
50. Zevgolis, A.; Wood, B. C.; Mehmedović, Z.; Hall, A. T.; Alves, T. C.; Adelstein, N., Alloying effects on superionic conductivity in lithium indium halides for all-solid-state batteries. *APL Materials* **2018,** *6* (4), 047903.
51. Ohno, S.; Banik, A.; Dewald, G. F.; Kraft, M. A.; Krauskopf, T.; Minafra, N.; Till, P.; Weiss, M.; Zeier, W. G., Materials design of ionic conductors for solid state batteries. *Progress in Energy* **2020,** *2* (2), 022001.
52. Muy, S.; Bachman, J. C.; Chang, H.-H.; Giordano, L.; Maglia, F.; Lupart, S.; Lamp, P.; Zeier, W. G.; Shao-Horn, Y., Lithium Conductivity and Meyer-Neldel Rule in Li3PO4–Li3VO4–Li4GeO4 Lithium Superionic Conductors. *Chem. Mater.* **2018,** *30* (16), 5573-5582.
53. Metselaar, R.; Oversluizen, G., The meyer-neldel rule in semiconductors. *J. Solid State Chem.* **1984,** *55* (3), 320-326.
54. Sebti, E.; Qi, J.; Richardson, P. M.; Ridley, P.; Wu, E. A.; Banerjee, S.; Giovine, R.; Cronk, A.; Ham, S.-Y.; Meng, Y. S.; Ong, S. P.; Clément, R. J., Synthetic control of structure and conduction properties in Na–Y–Zr–

Cl solid electrolytes. *Journal of Materials Chemistry A* **2022,** *10* (40), 21565-21578.

For table of contents only

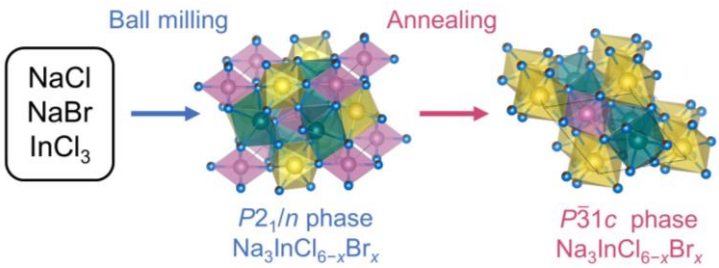

Synopsis

A series of halide mixed solid solutions of $Na_3InCl_{6-x}Br_x$ ($0 \leq x \leq 2$) is successfully synthesized. By mechanical milling, the $Na_3InCl_{6-x}Br_x$ solid solution series adopts a monoclinic $P2_1/n$ phase, while the subsequent annealing transforms it into a trigonal $P\bar{3}1c$ phase.